CuO/ZnO Nanocorals synthesis via hydrothermal technique: growth mechanism and their application as Humidity Sensor

Ahmed Zainelabdin, Gul Amin, Siama Zaman, Omer Nur, Jun Lu,
Lars Hultman and Magnus Willander

Original Publication:

Ahmed Zainelabdin, Gul Amin, Siama Zaman, Omer Nur, Jun Lu, Lars Hultman and Magnus Willander, CuO/ZnO Nanocorals synthesis via hydrothermal technique: growth mechanism and their application as Humidity Sensor, 2012, Journal of Materials Chemistry, (22), 23, 11583-11590.
http://dx.doi.org/10.1039/c2jm16597j

CuO/ZnO Nanocorals synthesis via hydrothermal technique: growth mechanism and their application as Humidity Sensor

A. Zainelabdin,[1*] G. Amin,[1] S. Zaman,[1] O. Nur,[1] J. Lu,[2] L. Hultman,[2] and M. Willander[1]

[1] Department of Science and Technology (ITN), Linköping University, SE-601 74 Norrköping, Sweden

[2] Department of Physics, Chemistry, and Biology (IFM), Linköping University, SE-581 83, Linköping, Sweden.

Abstract

We demonstrate hydrothermal synthesis of coral-like CuO nanostructures by selective growth on ZnO nanorods (NR) at low temperatures. During the hydrothermal processing the resultant hydroxylated and eroded surface of ZnO NR becomes favorable for the CuO nanostructures growth via oriented attachments. Heterojunction p-n diodes fabricated from the CuO/ZnO nanocorals (NC) reveal stable and high rectification diode properties with a turn-on voltage ~1.52 V and negligible reverse current. The humidity sensing characteristics of the CuO/ZnO NC diodes exhibit a remarkable linear (in a semilogarithmic scale) decrease in the DC resistance by more than three orders when the relative humidity is changed from 30 – 90 %. The NC humidity sensor is also found to reveal the highest sensitivity factor ~6045 among available data for the constituent material's and a response and recovery time of 6 s and 7 s, respectively.

KEYWORDS: Zinc oxide nanorods, copper oxide nanostructures, nanocorals, relative humidity, sensitivity factor.

Corresponding author email: ahmza@itn.liu.se

1. Introduction

One-dimensional (1-D) metal oxide (MO) nanostructures have attracted much attention in fabricating unique optoelectronic, electronic, and electrochemical devices such as UV sensors [1], solar cells [2], and gas sensors [3]. It pertains to those applications that nanorods possess relatively large aspect ratio and relatively large surface area to volume ratio ensuring high efficiency and sensitivity. As for materials of choice, zinc oxide (ZnO) is an environmentally-friendly n-type semiconductor that has better electron mobility compared to other wide band gap oxides including TiO_2[4]. Therefore, ZnO is expected to exhibits faster electron transport with reduced recombination loss. Different types of ZnO nanostructures have been used as gas sensors to detect gases, vapors, and metal ions, such as ethanol [3, 5], NH_3 [6], O_2 [7], and Ca^+ [8].

Likewise, CuO is an important p-type semiconductor with a narrow band gap (1.2 eV). CuO has been intensively studied for sensing devices due to its rich family of nanostructures and promising electrochemical and catalytic properties[8-11]. Previously reported CuO nanostructures are grown on Cu substrate using thermal oxidation process or synthesized through wet chemical routes on other supporting substrates like glass. However , CuO nanostructures (NS) grown by the later method showed poor adhesion to the substrates [11]. In recent years, the simple and cost effective hydrothermal method has proven to be successful for the synthesis of nanostructures of CuO or ZnO [12, 13]. By combining the advantages of both nanostructures in a composite simple, reliable and cost effective synthesis route might be realized.

Many combinations of CuO and ZnO nanostructures have been demonstrated, but involve high temperature (>500 ^oC) to oxidize a Cu foil into CuO followed by the deposition of ZnO [14]. Furthermore, Jung, S. et al [15] recently demonstrated the fabrication of flower-like CuO-ZnO nanowire heterostructures by photochemical deposition, which is a slow and rather expensive process.

Humidity sensing is increasingly important in areas, such as control systems for industrial processes, human comfort, and health. For most modern delicate devices, good control over the atmospheric conditions is necessary to avoid their fast degradation, e.g., at too dry environment these devices are susceptible to damage by discharge [16]. Therefore, a variety of humidity sensors have been developed mainly based on MO. The most common heterocontact system, CuO/ZnO, is extensively investigated due to their unique humidity-sensing characteristics, and also for detecting both CO and H_2 gases[17-19]. Most of the previously studied CuO/ZnO heterocontacts humidity sensors were fabricated by direct mechanical pressing of sintered MO with uneven and thick enough surfaces to avoid cracks or pinholes, resulting in poor humidity performance. Another method to fabricate humidity sensors is to deposit CuO on polycrystalline ZnO substrate [20], which however, is expensive and compromises the reproducibility of the physical heterocontacts.

The mechanism by which the CuO/ZnO heterojunction atmospheric sensor is working can be explained as follows. The sensor exhibits a well-defined rectifying behavior conventionally confirmed by the current-voltage characteristics of CuO/ZnO. When the heterocontact is intentionally exposed to the targeted atmospheric conditions, the chemical species to be detected in the surroundings can permeate into the interface of the p-n heterojunction; as a result the electrical properties of the heterojunction will vary in response to the species[21, 22].

By applying the hydrothermal approach we were able to precisely gain control over the synthesis of the nanocorals (NC) consisting of p-type CuO/n-type ZnO at low temperature. This is achieved by first growing ZnO nanorods, followed by assembling hierarchical CuO NC from a single-precursor entity (copper nitrate) at 60 ^{o}C. The nanohybrid device fabricated from these NC demonstrated an excellent rectifying diode behavior; because of their electrical characteristics together with their relatively large surface area. We have explored the impact of

the relative humidity on the NC sensor. An improved humidity sensing capability was reproducibly obtained. The results obtained from more than fours different NC sensors produced using the same procedure were consistent, indicating a potential for high reproducibility. Based on our knowledge; this is the first time that an inexpensive and easily synthesized CuO/ZnO NC heterojunction device is utilized as a humidity sensor.

2. Experimental

The synthesis of CuO/ZnO NC is performed by applying the widely known hydrothermal method for ZnO nanorods (NR) growth. The ZnO NRs were grown first through a two-step process. The first was a seed layer (ZnO nanoparticles) deposition followed by ZnO NR growth following the procedure described in [23]. In brief ZnO nanoparticles seed solution was spun coated three times on indium tin oxide (ITO) substrate. In the second step, an aqueous solution of a 50 mM [Zn $(NO_3)_2$. $6H_2O$] and 50 mM of hexamethylenetetramine (HMT) [$(C_6H_{12}N_4)$] was prepared to serve as precursor solution for the growth. The coated substrate was immersed in the precursor solution and loaded to an ordinary oven held at 50 ^oC for 6-8 h [23]. After the reaction was completed, the grown ZnO NR were carefully cleaned with deionized water and ethanol to remove residual salt and dried in air. For the growth process of CuO nanostructures, the freshly grown NR substrate was submerged having face up in a 5 mM aqueous solution of [$Cu(NO_3)_2$. $3H_2O$], and then heated to 60 ^oC for 1.5 - 4 h.

In order to fabricate a humidity sensor, the CuO/ZnO NC structure grown on an ITO substrate for 4 h was chosen. Three additional steps were performed to complete the preparation of the sensor. First, polystyrene (PS) was spin coated to insulate the hydrothermally grown ZnO NR, followed by reactive ion etching (RIE) to expose 2/3 for the second CuO nanostructures growth. Second, the as-prepared CuO/ZnO NC structures were coated again with

PS and RIE etched to uncover part of them for metallization with Au contacts. Third, a 100 nm thickness Au contacts were thermally evaporated through a shadow mask with a diameter of 1.5 mm for the subsequent electrical measurements.

3. Results and Discussion

The ZnO NR grown in the first hydrothermal process are shown in the scanning electron microscopy (SEM) image of Fig. 1a. Because of the nanoparticles coating substrate, the NR are mostly aligned normal to the substrate surface. It is widely accepted that ZnO nanoparticles reduce the hydrothermal barrier between heterogeneous materials by introducing favorable nucleation sites, which promotes vertical growth of aligned ZnO NR on the substrate surface. The ZnO NR has a typical length of around 1.5 μm and a diameter of around 80-120 nm. The second hydrothermal procedure yields highly branched CuO nanostructures that are selectively deposited on the ZnO NR as can be seen in Fig. 1b for samples grown at 60 ^{o}C for 1.5 h. The CuO leaf like nanostructures have dimensions of around 500 nm in length, 150 nm in width, and 70 nm in thickness. Interestingly at short growth time the CuO branches emerge from the sidewalls of ZnO NR, which act as a stem for this structure (inset of Fig. 1b). For growth experiment during 4 h, the CuO branches grow exclusively on the ZnO NR as shown in the SEM images of Fig. 1c-f. Furthermore, Fig. 1c also confirms the selective growth nature; as the empty places in the first hydrothermal growth (ZnO NR) apparently remained blank without any growth of CuO. The top and side view of the NC is shown in the SEM images of Fig. 1d-e. As evident, the CuO branches are now decorated by numerous nanoleaves that were densely packed on the ZnO NR. A representative SEM image of a single NC is shown in Fig. 1f. It is clear that the CuO nanostructures cover the entire surface of the ZnO NR after 4 h of hydrothermal growth. Growth more than 4 h results in a complete chemical dissolution of ZnO NR. As a consequence, there is

no stem for the CuO nanostructures, which can easily wash out during the cleaning process. However, in 4 h duration the entire ZnO NR surface roughen and become suitable to accommodate CuO nuclei as discussed above.

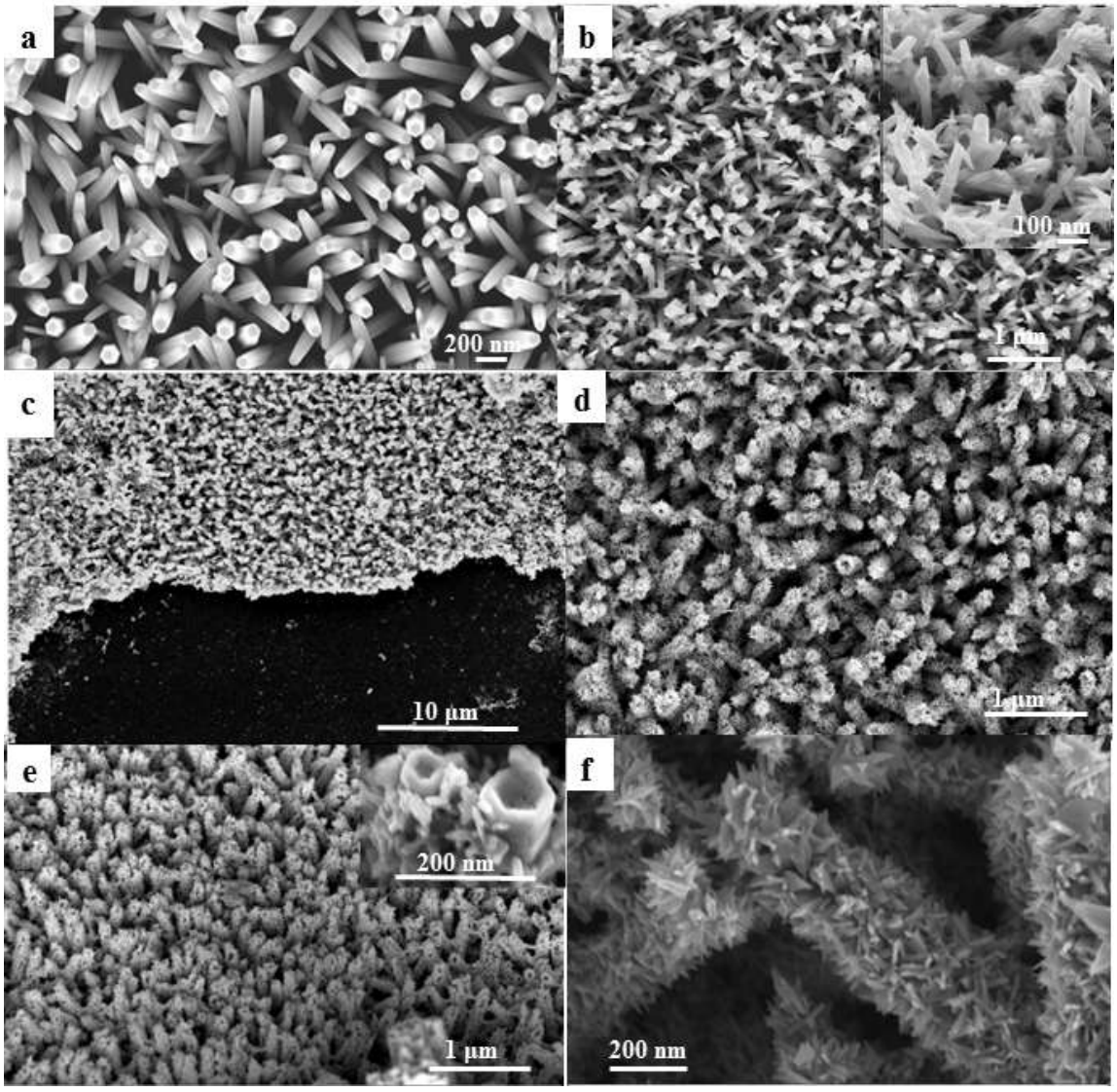

Figure 1: SEM images of (a) ZnO NR hydrothermally grown at 50 ^{o}C on ITO substrate for 6 h. CuO nanostructures (b) grown on ZnO NR for 1.5 h, inset shows a magnified image of CuO nanostructures grown on the sidewalls of ZnO NR (scale bar 100 nm). The CuO/ZnO NC are shown in (c) low magnification SEM where CuO assembled only on ZnO NR, (d-e) top and side view of the highly branched NC, the inset in (e) demonstrate the etching effect on ZnO NR tips, and (f) a single CuO/ZnO NC after hydrothermal growth for 4 h.

The crystal structures obtained were investigated by X-ray powder diffraction (XRD). Figure 2a shows the XRD pattern of bare hexagonal wurtzite ZnO NR (black curve), which were used as templates for growing the NC. The blue curve shows the diffraction pattern of CuO/ZnO NC with peaks from CuO and ZnO. The NC sample exhibited two main peaks of monoclinic CuO located at 2θ values of 35.5^{o} and 38.7^{o} that correspond to $(\bar{1}11)/(002)$ and (111)/(200) planes, respectively. The broadening and weakness of these peaks can be attributed to the small grain size and poor crystallinty of the CuO as discussed below. The peaks appearing at 31.8^{o}, 34.4^{o} and 36.2^{o} can be perfectly indexed to (100), (002), and (101), respectively, of the wurtzite phase ZnO according to the (JCPDS card No. 36-1451). The XRD pattern of the branch-grown CuO sample is shown in the inset of Fig. 2a (JCPDS card No. 05-0661). No peak related to of Cu, $Cu(OH)_2$ or Cu_2O phases was observed.

The CuO/ZnO NC were further investigated with transmission electron microscopy (TEM) and high-angle annular dark field imaging in scanning transmission electron microscopy (HAADF/STEM) with energy dispersed X-ray spectroscopic (EDS) for samples grown during 1.5 h. Fig 2b shows a low-magnification TEM image of a single ZnO NR with a number of CuO nanoleaves attached to it. The etching effect on the NR is visible on the tip (Fig. 2c) and sidewalls of the ZnO NR as evidenced more clearly by high resolution TEM (HRTEM) image shown in the inset of Fig. 2d, where 4- 8 nm notches were formed during the secondary CuO growth. A HRTEM image of the ZnO stem is presented in Fig. 2c showing that the preferred growth direction of the NR is along the [0001] direction in agreement with the XRD pattern. Enlarged TEM views of CuO nanoleaves adhered to the ZnO NR are shown in Fig. 2 (d) and (e). In (d) there are two interpenetrated nanoleaves having a length of ~ 150 nm and a diameter of ~ 60 nm. Each nanoleaf exhibits a rough surface as visible in Fig. 2d-e. The roughness behavior

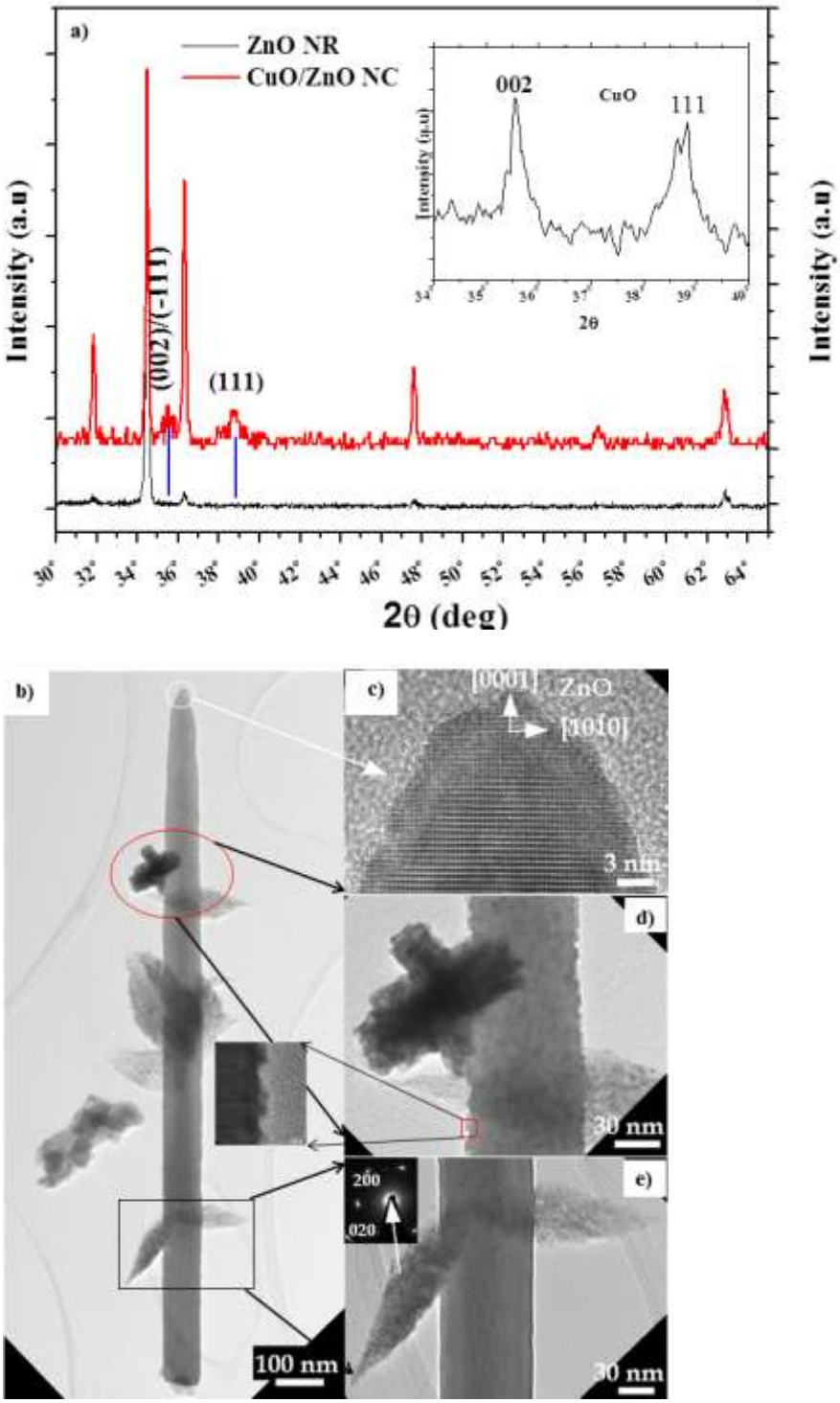

Figure 2: a) X-ray diffraction patterns of ZnO NR (black curve) and CuO/ZnO NC (blue curve) hydrothermally grown for 4 h, the inset shows CuO XRD peaks, (b) a TEM image of single ZnO NR with CuO nanoleaves, the inset shows a HRTEM image of the sidewall of ZnO NR, (c) HRTEM image of the ZnO NR with [0001] growth direction indicated, (d) and (e) a magnified TEM images of the red oval and black box in (b), a CuO nanoleaves with the corresponding SEAD pattern.

indicates that the nanoleaves are assembled from small CuO nanocrystals. The inset of Fig. 2e shows the selected area electron diffraction (SEAD) pattern of the CuO nanoleaf. The SEAD pattern reveals that the leaf is effectively a single crystal with the preferred growth direction along [010]. The slightly elongated diffraction spots show that the CuO nanoleaves consist of multiple nanodomains with a limited misorientation deviation. The slight misorientation can be observed in the high magnification TEM images (see Fig. 2d-e) showing a non-uniform contrast of the CuO grains. According to the TEM results we conclude that the CuO nanoleaves are built up of small nanocrystals 3-5 nm in size with almost the same crystal orientation. These results are consistent with published reports [24-26]. Moreover, SAED patterns from other CuO grains show a random orientation distribution between the CuO grains, which agrees well with the XRD pattern in Fig. 2a.

The weak acidic nature of the secondary growth solution (pH = 5.17) explains the CuO nanostructures growth behavior, since under such pH environments the ZnO NRs are slowly etched [27]. The etching effect is higher on top of the ZnO NR, as seen in the inset of Fig. 1e, compared to bottom since the top surface of the NR is exposed to the solution more as compared to the bottom. The density of the ZnO NR on the bottom of the substrate is also observed to be higher than that on top, which may protect the NR from the influence of the solution. The eroded surface of the ZnO NR, on the one hand, is highly reactive due to the presence of large defect (oxygen vacancies) densities [28] where dissociative adsorption of water molecules are more favorable, resulting in high local pH (OH^- concentration) in the vicinity of the defective ZnO NR. As a consequence, the irregular and rough surface of ZnO NR serves to nucleate the CuO. The HAADF /STEM of the CuO/ZnO NC grown for 1.5 h is shown in Fig. 3a. The EDS line scan (not shown here) was performed along the white line shown in Fig. 3a. The ZnO NR in this sample is expected to be partly covered by CuO. Indeed the HAADF/STEM image of Fig. 3a

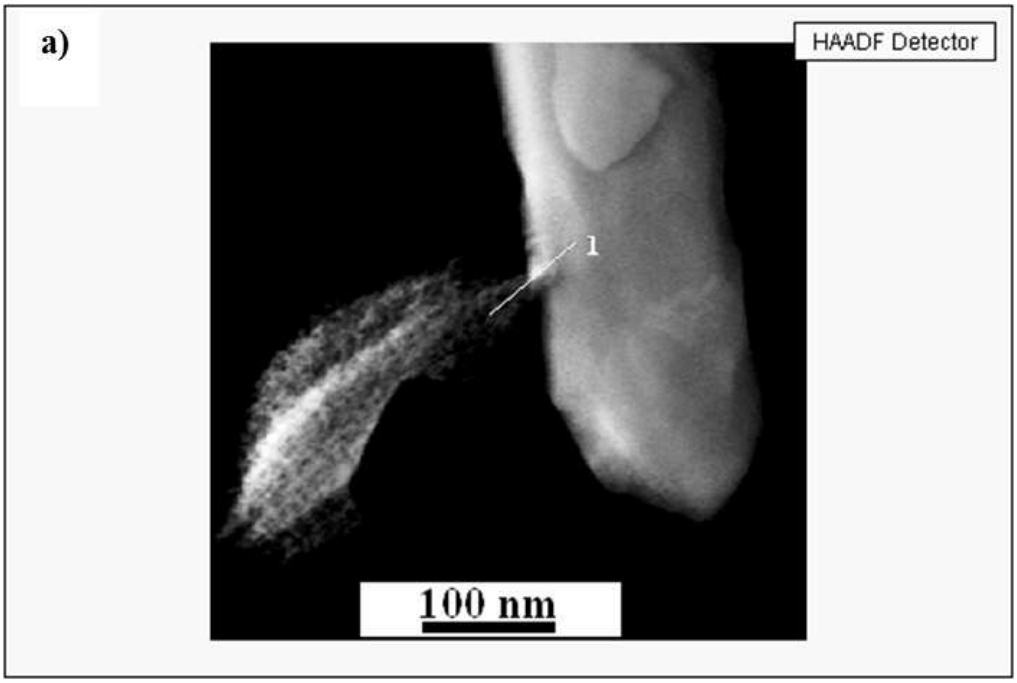

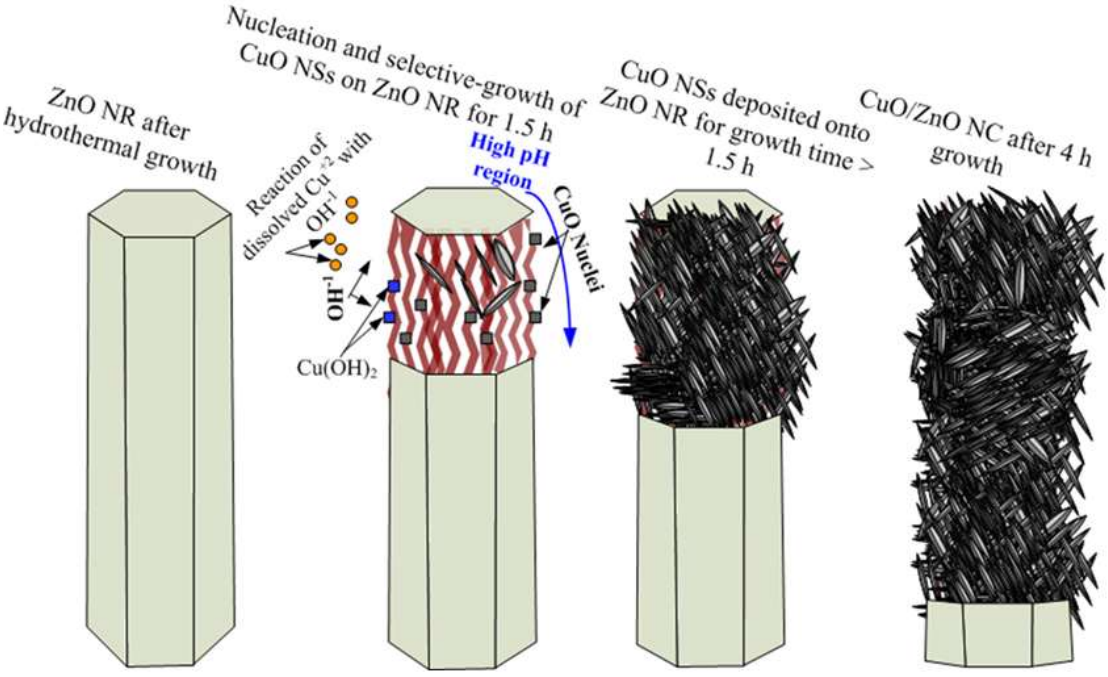

Figure 3: a) The HAADF/STEM image of the CuO/ZnO nanostructures grown for 1.5 h, (b) Schematic diagram of the growth steps occurring in the secondary growth solution, and the effect of acidic condition on the ZnO NR and the hydroxylation-dehydroxylation processes.

indicated that the ZnO NR is partly covered by the CuO. However, no uniform coverage was found. For samples grown for much longer duration the CuO is expected to cover much larger surface of the ZnO nanorods. It is important to note that the contrast of the HAADF/STEM imaging depends on the square of the atomic number. Since the present system is composed of two materials with atomic numbers (Z^2) very close to each other (for Zn, Z=30, and Cu, Z=29) it is difficult to separate atoms of Cu residing on the surface of the ZnO NR.

The schematic diagram of Fig. 3b summarizes the growth mechanism of CuO/ZnO NC based on the SEM and TEM results. Under the low pH precursor solution used to synthesize the CuO nanostructures, the surface of ZnO NR is etched giving rise to dissociative adsorption of water on the defective ZnO NR surface [28]. As a consequence a rough and hydroxylated ZnO NR surface is produced with high local pH value in the vicinity of the NR. The locally produced OH^- will then react with the dissolved Cu^{+2} ions to form the intermediate $[Cu(OH)_2]$ aggregates [29]. The intermediate $[Cu(OH)_2]$ in turn becomes dehydrolyzed forming CuO nanoparticles [30], which are adsorbed into the notches already existing on the ZnO NR surface. As the growth continues the CuO nanoparticles attach to each other to form the CuO nanoleaf by the oriented attachment with low-angle grain boundaries[24]. Finally, the NC is constructed as shown in Fig. 3b by the continued growth of nanoleaves, and the ZnO NR is barely visible.

The findings on the growth can be used to fabricate p-n heterojunction based on CuO/ZnO NC for various potential applications such as photovoltaics and sensors. The CuO/ZnO NC hydrothermally grown for 4 h Fig. 1c-f were exploited to fabricate a humidity sensor. The CuO/ZnO NC showed in Fig. 1f offer two important features that are not available in the NC grown for 1.5 h Fig.1b. First the high porosity of CuO/ZnO NC grown for 4 h makes the material apt to absorb water molecules by means of the capillary condensation [31]. The other feature is the

large surface areas of the NC grown for 4 h, which increases the water uptake. Therefore, the novel CuO/ZnO NC is expected to exhibit an improved response to humidity variations.

The schematic diagram of the fabricated device i.e. depicting the various parts of the NC humidity sensor, as well as the sensing active area is illustrated in Fig. 4a. The current density-voltage (J-V) characteristics of the p-n CuO/ZnO NC heterojunction diode were studied by simulating the lab conditions at temperature of 25 ^{o}C and RH of ~ 52 % inside an environmental chamber connected to Agilent 4155B semiconductor parameter analyzer. Figure 4b shows the typical J-V characteristics of the p-n NC diode with obvious rectifying behavior. The turn-on voltage was found to be 1.52 V, which is similar to 1.55 V reported for sputtered CuO thin film onto ZnO polycrystalline substrates[20]. The Ohmic contacts characteristics of the (Au/CuO/ZnO NC /ITO) were measured at room temperature by the parameter analyzer and the results are shown in the inset of Fig. 4b. It is evident that both Au and ITO demonstrate excellent and low contact resistance properties to the CuO/ZnO NC. Hence, the observed rectification of the diode is primarily comes from the p-n heterojunction. Interestingly, the NC p-n diode showed negligible reverse current and reasonably high rectification factor of 320 at ± 3 V.

The fabricated CuO/ZnO NC p-n heterojunction diode was inserted into a Blue M electric environmental chamber (a Signal General company) where the temperature was held constant at 25 ^{o}C while the relative humidity (RH) was varied from 30% to 90 % in steps of 5%. The NC sensor rapidly responded to small changes in the RH, but we allowed a 20 minutes period after the desired RH value was reached in order to ensure that the absorbed water was equilibrated with the vapor phase. The current density-voltage characteristics of the NC device under various RH are shown in Fig. 5. The forward current density J_F was increased by almost

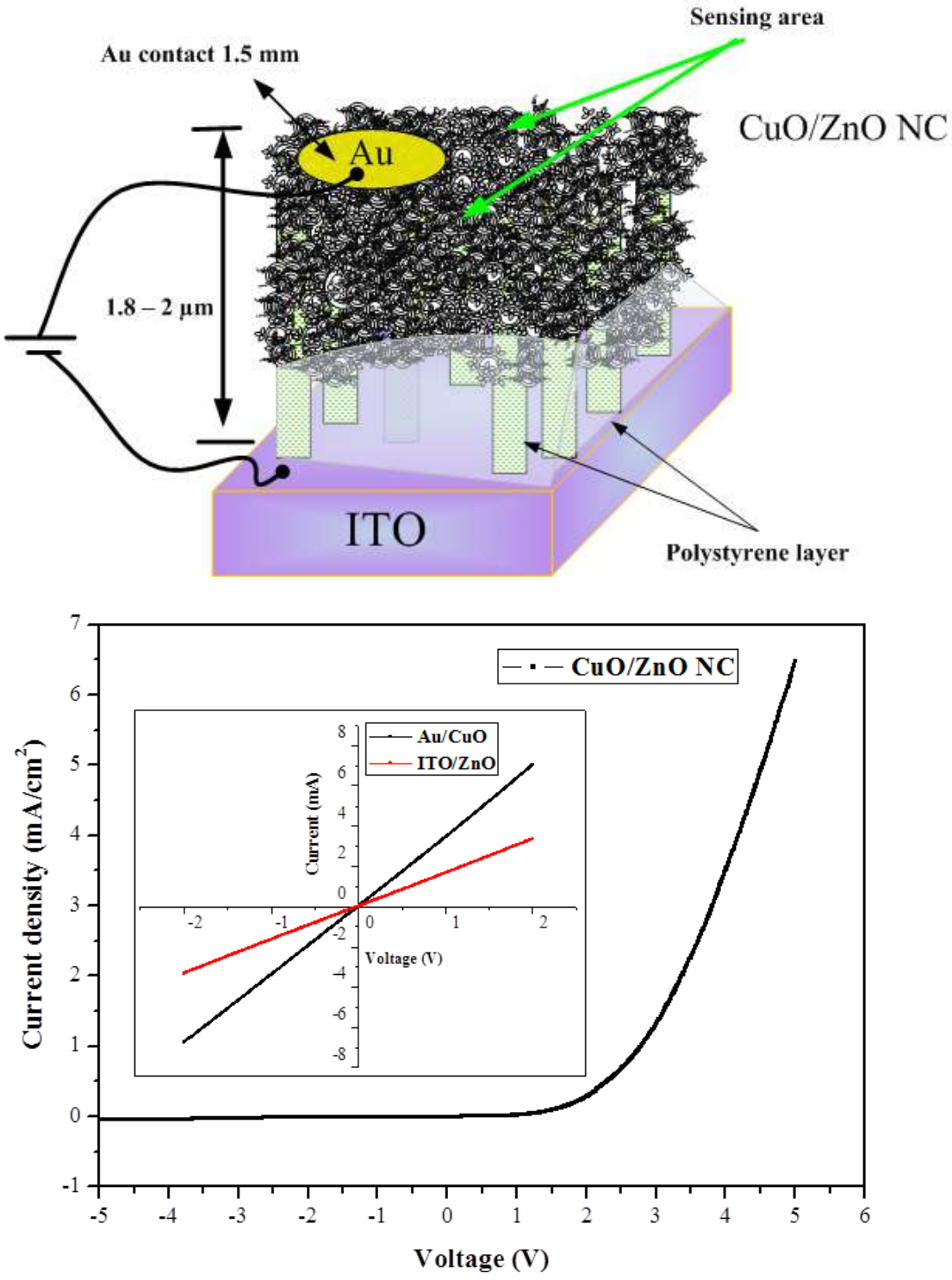

Figure 4: (a) Current density-voltage characteristics of a typical CuO/ZnO NC p-n heterojunction with rectifying behavior, inset shows Ohmic contacts behavior of Au and ITO to CuO and ZnO, respectively. (b) Schematic diagram of the fabricated CuO/ZnO NC humidity sensor.

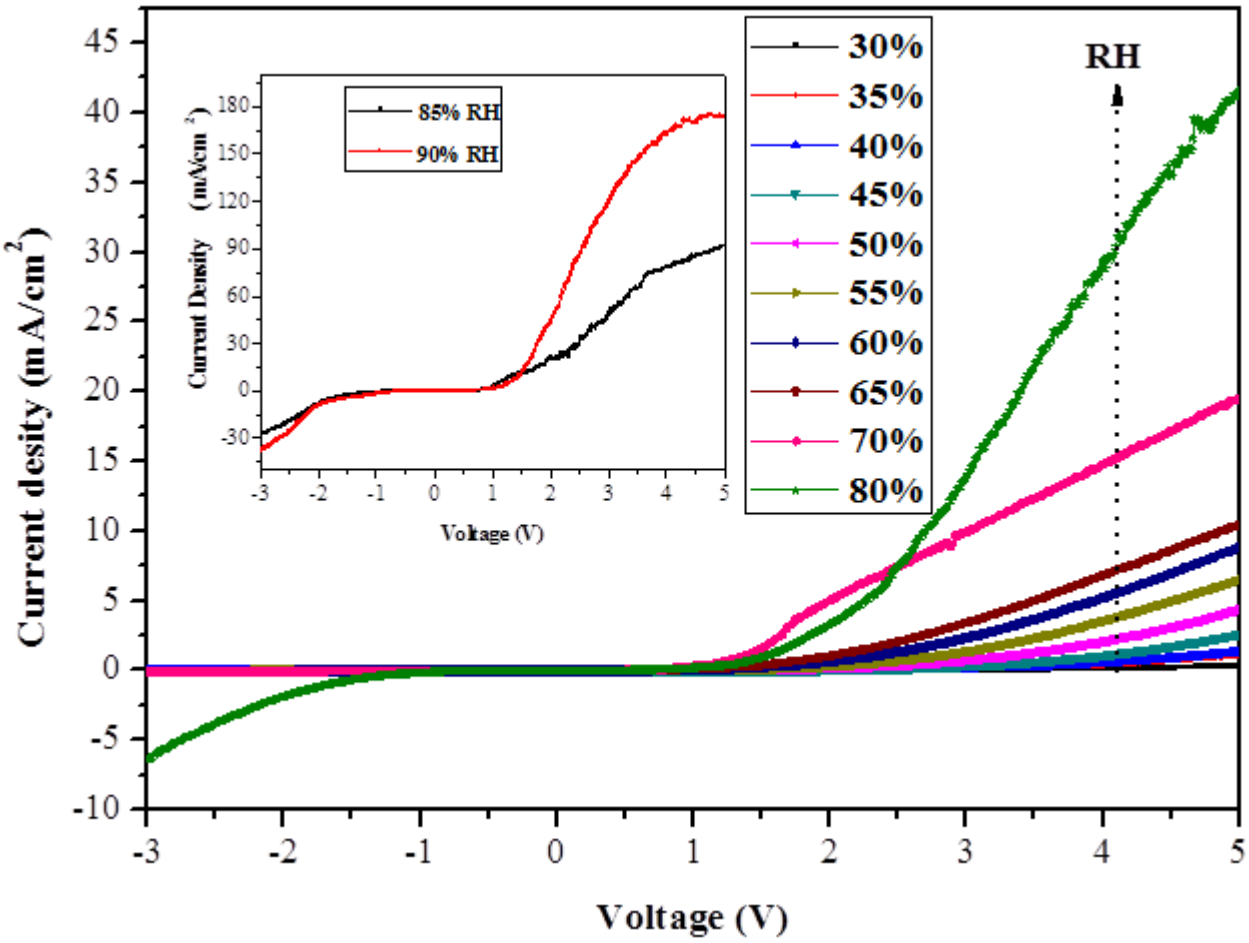

Figure 5: Current density- voltage characteristics of a typical NC sensor at different relative humidity (RH), inset shows the J-V characteristics of the sensor at 85 and 90 % RH.

four orders of magnitude when the RH was varied from 30% to 90%, while the reverse current density J_R was almost independent on the RH up to 70 %. The J_R starts to increase noticeably with RH above 70% as shown in the inset of Fig. 5, where the RH at 85 % and 90 % are plotted separately to reveal their J_R variations with RH. The results of the DC resistance for the NC sensor biased at 1.6 V (above the turn on) as a function of RH at 25 ^oC are presented in Fig. 6a. It is evident that the sensor resistance drops almost linear on a semilogarithmic scale with increasing RH by approximately three orders of magnitude (10^6–10^3), demonstrating an excellent sensor linearity and sensitivity over a wide range of RH. The sensitivity factor[32] S_f (known as

$R_{30\%}/R_{90\%}$) is found to be 6045 (± 731), which is significantly higher than the reported S_f values of individual nanomaterials junction (CuO or ZnO). For comparison, ZnO nanorods and nanowire humidity sensors reported in [32] have sensitivity factors S_f = 183 and 5442, respectively. Honeycomb-like CuO exhibits a S_f value of only 130 even though a wider RH range was used [33]. Therefore, our current CuO/ZnO NC sensor represents a simple and excellent candidate for RH measurements. The reproducibility of the sensing was tested using four different sensors fabricated using the same process. The standard deviation shown above is 12%. This is rather high but it is explained by the different density of ZnO NR and/or the CuO nanostructures on each of the tested samples. An important point is that the NC sensor shows relatively high hysteric behavior of about 21% upon performing recovery cycles of the RH from 90% to 30% Fig. 6a. This implies that there are surface reactions preventing water desorption from the NC pores and thus influencing the sensor response. Therefore, the present sensor requires modifications such as introduction of inter-digitized electrodes, packaging, and connecting the device to a heater to restore the NC sensor responsivity prior to RH measurements. Figure 6b shows the dynamic response of the NC sensor to rapid variations in the RH range between 32% and 96%. The sensor was switched back and forth between two sealed chambers containing a saturated solution of $MgCl_2$ and KNO_3 with RH values of 32% and 96 %, respectively [34]. The time taken by a sensor to reach 90% of the total impedance change is defined as the dynamic response time in both cases of water adsorption or desorption [32]. The response time and recovery time of the present NC sensor were about 6 s (± 1) and 7 s (± 0.6 s), respectively, demonstrating that the present NC sensor is rapidly responding to the ambient RH. As compared with other CuO/ZnO RH sensor published before, e.g.[21], the present CuO/ZnO NC demonstrated comparatively large S_f value and relatively wider RH operation range. The CuO/ZnO nanoparticles RH sensor reported before, exhibited high response only at RH ranges > 50 % [21],

while the present sensor performance show high response for RH down to 30%. The present CuO/ZnO NC RH sensor also has fast response and recovery times of 6 s and 7s as compared to that of 40 s and 50 s for the CuO-ZnO nanoparticle RH sensor [21]. However, the CuO/ZnO NC RH sensor shows relatively large historic effect 21 % as compared to 4 % reported in [21], which implies that the NC RH sensor requires further optimization regarding the design of the sensor.

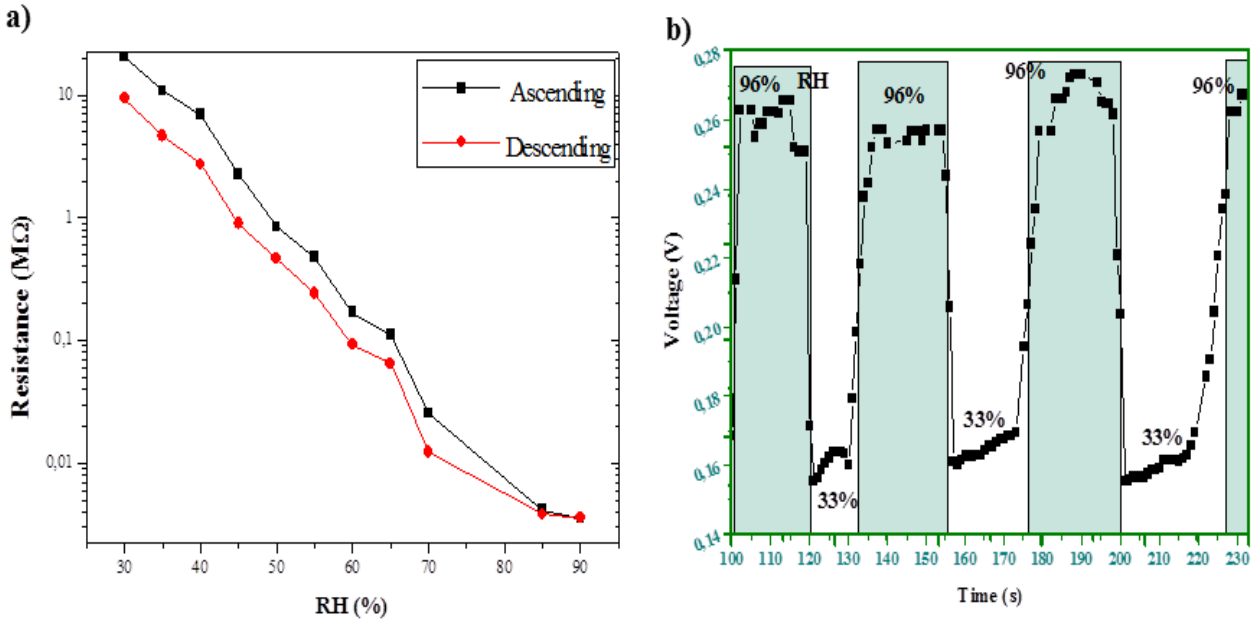

Figure 6: DC resistance (a) of a typical NC sensor with increasing humidity and recovery cycle (ascending and descending), and dynamic response (b) of the NC sensor when switched between 96 % and 32 % RH.

The changes in the NC sensor resistance with RH variations can be explained from the recent review by Chen and Lu [35]. At low RH water chemisorb to the surface of a ceramic material resulting in the formation of two surface hydroxyls per water molecule (dissociative adsorption). Additional water molecules from the ambient will physically-adsorb to the previously formed hydroxyls groups forming a physisorbed monolayer. At this stage no proton conduction takes place due to inhibited motion. Furthermore, continuous water adsorption on the material surface will give rise to physisorbed water multilayers, which are less affected by the

underlying chemosorbed layer. Consequently, the protons will gain freedom to move inside the randomly oriented physisorbed water multilayers according to the Grotthuss mechanism [35]. Based on this model and our previous discussion about water dissociation on defects presented on the surface/interface of hydrothermally grown oxides[28, 36], one can explain the efficient RH response of the NC sensor. As the CuO/ZnO NC were grown at low temperature, hence the presence of a high density of interface states is expected. Thus, the carrier transport at the p-n junction sites of the NC heterojunctions under forward bias conditions is likely due to both the pinning of the Fermi level by the interface states and the injected current [35]. The high sensitivity of the NC sensor to the RH variation can thus be explained in terms of the saturation of these interface states by the physisorbed water. The higher the RH, the higher the amount of water molecules on the p-n junction surfaces, and thus the larger the number of trapped electrons released, resulting in an increase in the forward current [35]. Under high RH levels electrolysis of adsorbed water takes place at the NC heterojunction sites[16]. The electrolysis process can be understood as follows, at high RH the amount of adsorbed water increases on the NC heterojunction sites. In the vicinity of the p-n junction, holes are injected from the CuO into the adsorbed water, giving rise to protons in the adsorbed water. This positive charge is released at the surface of the ZnO and thus electrolyzes the adsorbed water [16, 35].

4. Conclusion

In conclusion, a simple and cost efficient hydrothermal approach was utilized to synthesize CuO/ZnO NC at low temperatures. The branched CuO demonstrate strong selectivity to ZnO NR with growth starting on the sidewalls of the ZnO NR. The acidic conditions of the CuO precursor solution make the surface of the ZnO NR become rough and defective, which in turn promote the oriented growth of CuO nanostructures. p-n heterojunction diodes fabricated using these NC demonstrate an excellent characteristics with high rectification factor. The

fabricated NC sensor exhibits remarkable humidity sensing properties, where the DC resistance of the sensor is greatly influenced by the ambient humidity and decreases by more than three orders of magnitude over a measured RH range. The NC sensor also demonstrates fast dynamic response to humidity variations together with the highest sensitivity factor S_f reported for its constituent nanomaterials. The sensor thus carries great potential for humidity-sensing applications in many fields such as industrial control processes, medical, and life-related applications with low-cost and simple methods.

Acknowledgement:

The financial support from the Swedish government strategic research area grant in materials science, Linköping University is appreciated.

References

1. J. M. Seminario, A. J. Gimenez and J. M. Yanez-Limon, *Journal of Physical Chemistry C*, 2011, **115**, 282-287.

2. Q. Zhang and G. Cao, *Nano Today*, 2011, **6**, 91-109.

3. J. Yi, J. M. Lee and W. I. Park, *Sensors and Actuators B: Chemical*, 2011, **155**, 264-269.

4. S. H. Ko, D. Lee, H. W. Kang, K. H. Nam, J. Y. Yeo, S. J. Hong, C. P. Grigoropoulos and H. J. Sung, *Nano Lett*, 2011, **11**, 666-671.

5. S. Choopun, A. Tubtimtae, T. Santhaveesuk, S. Nilphai, E. Wongrat and N. Hongsith, *Appl Surf Sci*, 2009, **256**, 998-1002.

6. J.-M. Tulliani, A. Cavalieri, S. Musso, E. Sardella and F. Geobaldo, *Sensors and Actuators B: Chemical*, 2011, **152**, 144-154.

7. Y. Hu, J. Zhou, P.-H. Yeh, Z. Li, T.-Y. Wei and Z. L. Wang, *Advanced Materials*, 2010, **22**, 3327-3332.

8. M. H. Asif, A. Fulati, O. Nur, M. Willander, C. Brannmark, P. Stralfors, S. I. Borjesson and F. Elinder, *Appl Phys Lett*, 2009, **95**, 023703-023703.

9. M. Faisal, S. B. Khan, M. M. Rahman, A. Jamal and A. Umar, *Materials Letters*, 2011, **65**, 1400-1403.

10. X. Jiang, W. Huang, H. Li and X. Zheng, *Energy & Fuels*, 2009, **24**, 261-266.

11. D. Li, Y. H. Leung, A. B. Djurisic, Z. T. Liu, M. H. Xie, J. Gao and W. K. Chan, *J Cryst Growth*, 2005, **282**, 105-111.

12. Z. L. Wang, Y. Qin and R. S. Yang, *Journal of Physical Chemistry C*, 2008, **112**, 18734-18736.

13. G. Gao, H. Wu, M. Chen, L. Zhang, B. Yu and L. Xiang, *J Electrochem Soc*, 2011, **158**, K69-K73.

14. Y. Zhu, C. H. Sow, T. Yu, Q. Zhao, P. Li, Z. Shen, D. Yu and J. T. L. Thong, *Adv Funct Mater*, 2006, **16**, 2415-2422.

15. S. Jung, S. Jeon and K. Yong, *Nanotechnology*, 2011, **22**, 015606.

16. B. M. Kulwicki, *Journal of the American Ceramic Society*, 1991, **74**, 697-708.

17. D. H. Yoon, J. H. Yu and G. M. Choi, *Sensors and Actuators B: Chemical*, 1998, **46**, 15-23.

18. M. Miyayama, K. Hikita, G. Uozumi and H. Yanagida, *Sensors and Actuators B: Chemical*, 1995, **25**, 383-387.

19. S. Aygün and D. Cann, *Sensors and Actuators B: Chemical*, 2005, **106**, 837-842.

20. K.-K. Baek and H. L. Tuller, *Solid State Ionics*, 1995, **75**, 179-186.

21. Q. Qi, T. Zhang, Y. Zeng and H. Yang, *Sensors and Actuators B: Chemical*, 2009, **137**, 21-26.

22. S. Aygun and D. Cann, *J Phys Chem B*, 2005, **109**, 7878-7882.

23. A. Zainelabdin, S. Zaman, G. Amin, O. Nur and M. Willander, *Crystal Growth and Design*, 2010, **10**, 3250-3256.

24. W. Z. Wang, H. L. Xu, W. Zhu, L. Zhou and M. L. Ruan, *Cryst Growth Des*, 2007, **7**, 2720-2724.

25. X. T. Huang, J. P. Liu, Y. Y. Li, K. M. Sulieman, X. He and F. L. Sun, *Cryst Growth Des*, 2006, **6**, 1690-1696.

26. S. H. Yu, Q. Zhang and S. J. Liu, *Journal of Materials Chemistry*, 2009, **19**, 191-207.

27. J. Zhou, N. S. Xu and Z. L. Wang, *Advanced Materials*, 2006, **18**, 2432-2435.

28. C. Woll, *Progress in Surface Science*, 2007, **82**, 55-120.

29. W. X. Zhang, Z. H. Yang, J. Xu, A. P. Liu and S. P. Tang, *Journal of Solid State Chemistry*, 2007, **180**, 1390-1396.

30. G. Van Tendeloo and G. H. Du, *Chemical Physics Letters*, 2004, **393**, 64-69.

31. T. Nitta and S. Hayakawa, *Ieee T Compon Hybr*, 1980, **3**, 237-243.

32. Z. Q. Zhu, Y. S. Zhang, K. Yu, D. S. Jiang, H. R. Geng and L. Q. Luo, *Appl Surf Sci*, 2005, **242**, 212-217.

33. K. Yu, J. W. Xu, J. Wu, D. J. Shang, L. J. Li, Y. Xu and Z. Q. Zhu, *Journal of Physics D-Applied Physics*, 2009, **42**.

34. L. Greenspan, *Journal of Research of the National Bureau of Standards Section a-Physics and Chemistry*, 1977, **81**, 89-96.

35. Z. Chen and C. Lu, *Sensor Letters*, 2005, **3**, 274-295.

36. O. Dulub, B. Meyer and U. Diebold, *Physical Review Letters*, 2005, **95**, 136101.